Filling the Gaps between Graphene Oxide: A General Strategy toward Nanolayered Oxides

Yoshitaka Saito, Xi Luo, Chunsong Zhao, Wei Pan, Chengmeng Chen, Jianghong Gong, Hidetoshi Matsumoto, Jie Yao, and Hui Wu**

Despite extraordinary developments in the research of 2D inorganic nanomaterials, a scalable and generalized synthetic method toward 2D oxide materials that lack layered lattice structures is still challenging. Herein, an easy and versatile solution-based route to synthesize oxides with layered nanostructures by combining sol–gel method with graphene oxide (GO) paper templates is reported. GO can stack together to form a paper-like membrane, the gap between two GO layers provides ideal 2D space to template the growth of oxide nanolayers. By this simple strategy, the gaps are filled successfully with polycrystalline TiO_2, ZnO, Fe_2O_3, and amorphous SiO_2 nanolayers with thickness of 1–5 nm. Single or multilayers of the oxide-based ceramic/glass nanolayers for applications in electronics, catalysts, energy storage, and gas separation can be expected; as an example, it is shown that layered Fe_2O_3 electrodes exhibit high performance for lithium-ion battery due to enhanced electrical connections between the 2D nanolayers.

1. Introduction

The field of 2D nanomaterials, which was triggered by the successes of graphene, has been enjoying extraordinary growth in recent years.[1–7] Inorganic compounds with 2D nanoarchitectures, which possess nanoscale thickness and infinite lateral dimensions,[5,8–11] are particularly important and interesting due to their exotic fundamental physical properties coming from anisotropy and nanosized effects which differ from their bulks.[11–17] Moreover, their unique magnetic, dielectric, catalytic, photochromic, photoluminescent, and conducting properties lead to numerous successful applications ranging from energy storage materials to molecular sieving.[13–20] With the rapid growth of the 2D nanomaterials research area, the scalable and controllable fabrication of 2D compounds naturally plays more and more important fundamental role.[3,8,21–24] To date, the most popular method to fabricate 2D inorganic nanomaterial is based on exfoliation from natural or artificial layer compound, such as MoS_2, WS_2, Bi_2Se_3, BN, carbide, black phosphorus, clay, and mica.[5,9–13,16,25–32] While significant attention has been drawn to the exfoliation method (including mechanical exfoliation, intercalation, electrochemical exfoliation and topochemical deintercalation), such strategy is not applicable to metal oxide materials that lack layered lattice structures.[10]

On the other hand, oxide materials, such as wurtzite ZnO, rutile and anatase TiO_2, tetragonal SnO_2, hematite Fe_2O_3, perovskite ABO_3 compounds ($BaTiO_3$, $BiFeO_3$, $BiVO_3$), amorphous SiO_2, and so on, have led to extensive application including energy conversion, environmental protection, and electronic devices in the past decades.[33] While such oxides with shrunk dimensions, for example highly confined thicknesses, provide opportunities for further exploring their physical properties and developing more applications, most functional oxides cannot be exfoliated from their bulk crystals to form a 2D nanostructure according to their nonlayered crystal structure. Engineering the dimensions of oxides that are not suitable for exfoliation methods is a challenge in the whole area of 2D nanomaterial research, and it is thus highly desirable to develop new and generalized strategies to tackle this challenging but very important problem.

Recently, Sun et al. reported a fundamental approach to molecular self-assembly synthesis of ultrathin 2D nanosheets of transition metal oxides by rationally employing lamellar reverse micelles.[21] While great success has been achieved to synthesize 2D oxides, current methods still need careful design of the surfactant systems and employing complex synthetic steps relying on the hydrothermal or solvothermal reactions.[11,29,30]

Y. Saito, X. Luo, C. Zhao, Prof. W. Pan, Prof. J. Gong, Prof. H. Wu
State Key Laboratory of New Ceramics and Fine Processing
School of Materials Science and Engineering
Tsinghua University
Beijing 100084, P.R. China
E-mail: panw@tsinghua.edu.cn; huiwu@tsinghua.edu.cn
Y. Saito, Prof. H. Matsumoto
Department of Organic and Polymeric Materials
Tokyo Institute of Technology
2-12-1 O-okayama, Meguro-ku, Tokyo 152-8552, Japan
Prof. C. Chen
Key Laboratory of Carbon Materials, Institute of Coal Chemistry
Chinese Academy of Sciences
27 Taoyuan South Road, Taiyuan 030001, P.R. China
Prof. J. Yao
Department of Materials Science and Engineering
University of California
Berkeley, CA 94720, USA

DOI: 10.1002/adfm.201501358

The sizes of the materials were also limited by the micelle size. Sol–gel method, on the other hand, provides us a new approach to substantially simplify such processes[34] Sol–gel-derived materials have been successfully used to fabricate not only bulks ceramic and glass, but also oxide materials in thin film, nanoparticle, and nanofiber structures.[34,35] We propose that sol–gel technique certainly holds great potential to process oxides with 2D nanoarchitectures. Here, we demonstrate the implementation of sol–gel method in developing a new family of low dimensional nanomaterials, including 2D oxides, with the introduction of a suitable 2D template that confines the growth of sol–gel-derived oxide materials. Graphene oxide (GO) papers with a large number of tiny 2D gaps are ideal templates for the growth of ceramic and glass nanolayers. We show that a series of precursor solutions can be driven into the gaps inside GO paper and form thin layered solids. Oxide nanolayers (ONLs) can be easily obtained by subsequently calcination. This synthetic route is simple and highly efficient to fabricate TiO_2, ZnO, Fe_2O_3, and SiO_2 nanolayers with thickness of 1–5 nm. In principle, this versatile method is not sensitive to the precursors used and can be applied to obtain 2D nanolayers of all inorganic materials that are suitable for sol–gel synthesis.

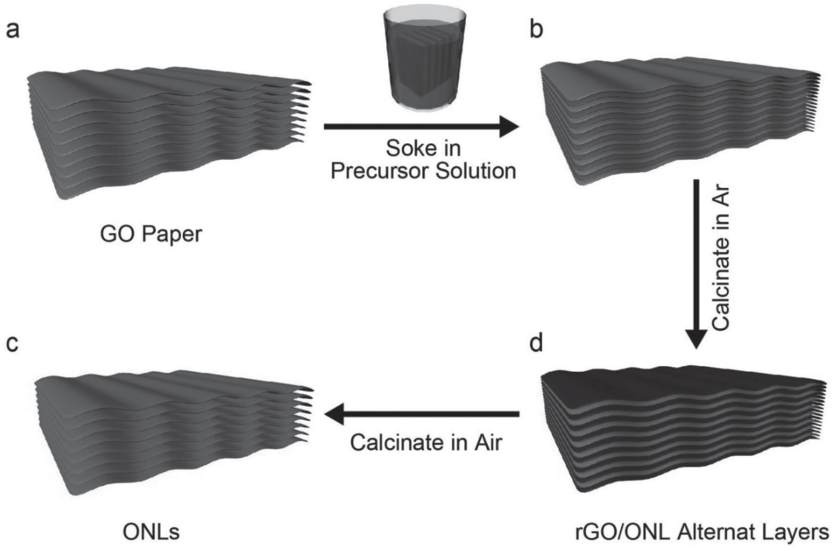

Figure 1. Schematic drawing of the synthetic method toward 2D oxide nanolayers. a) GO paper has been employed as starting materials. b) Dry GO paper has been immersed in a precursor solution, the solution wetted and filled the gaps between GO layers due to capillary force. The GO paper is dried after solution insertion, leaving solid precursor intercalated between GO layers. c) After heating in air atmosphere, oxide layers formed between rGO sheets. d) Layered 2D oxide sheets have been fabricated after removal of rGO by calcinations in air atmosphere.

2. Results and Discussion

2.1. Materials Design

GO is one of the most famous anisotropic 2D materials, which has been intensely studied because of its characteristic features (e.g., electrical, thermal, and mechanical properties) as with graphene.[21,23,36–42] As another interesting characteristic of GO, it can be easily stacked to form well-regulated layered structure (so-called GO sheet or GO paper) when its dispersed solution was filtered or dried.[36,39,43] GO papers have already attracted attention of many important cutting edge devices including super capacitor, solar cell, etc.[21,23,36–39] While intense studies have been focused on the functionalities of materials themselves in a GO paper, in this study, we take advantage of the rich empty gaps between GO layers (**Figure 1**). The width of these exceedingly high aspect-ratio 2D gaps is known to be about 0.80 nm at dry condition. Such 2D gaps naturally provide a flexible template for the synthesis of 2D solids while combined with sol–gel process.

2.2. Materials Synthesis

The synthesis of 2D oxide nanolayers typically follows the steps described in Figure 1. The GO membranes can be obtained by slow evaporation of GO solution or by the filtration method.[23,28,41,44] The material has exceptional stiffness and strength due to the intrinsic strength of the 2D graphene backbone.[23,37,42,44] Therefore, GO paper can be easily transferred and handled (Figure S1, Supporting Information). In the first step, GO paper was immersed in a metal oxide precursor solution overnight, the solution slowly infiltrated into the 2D gaps between GO layers by capillary force due to the hydrophilic nature[44] of GO (Figure S2, Supporting Information). The composite materials were then dried at 80 °C. Oxide precursor solid was filled in between GO sheets, which formed alternate layer-by-layer sheets of GO and oxide precursor solids (Figure 1b). Second, the dried membrane was annealed in argon atmosphere to convert oxide precursor into oxide crystals. After annealing, GO was reduced to reduced GO (rGO).[45] Figure S3 (Supporting Information) shows the X-ray diffraction (XRD) patterns, which indicate the change of the interlayer distance from 0.79 nm (GO) to 0.36 nm (rGO). Meanwhile, the precursor layers turns to oxide following a typical sol–gel reaction. Thus, the GO paper becomes a composite membrane with alternate layer-by-layer structure of rGO and oxide (Figure 1c). We emphasize that such layered rGO/oxide composite membrane in general is very interesting for further investigation in electrical, mechanical, thermal, and optical properties. However, in this study, in order to get pure oxide nanolayers, we removed the rGO layers by calcinations. As the third step (Figure 1d), the composite membrane was heated in air to above 600 °C to remove rGO; a thick film of stacked oxide layers can be generated subsequently. As an alternative route, the composite membrane of rGO and ONL can also be treated by sonication to separate the rGO and ONL. These separated layers were then calcinated in air atmosphere to get oxide layers as individual nanolayers. We synthesized TiO_2, ZnO, Fe_2O_3, and SiO_2 nanolayers following this synthetic

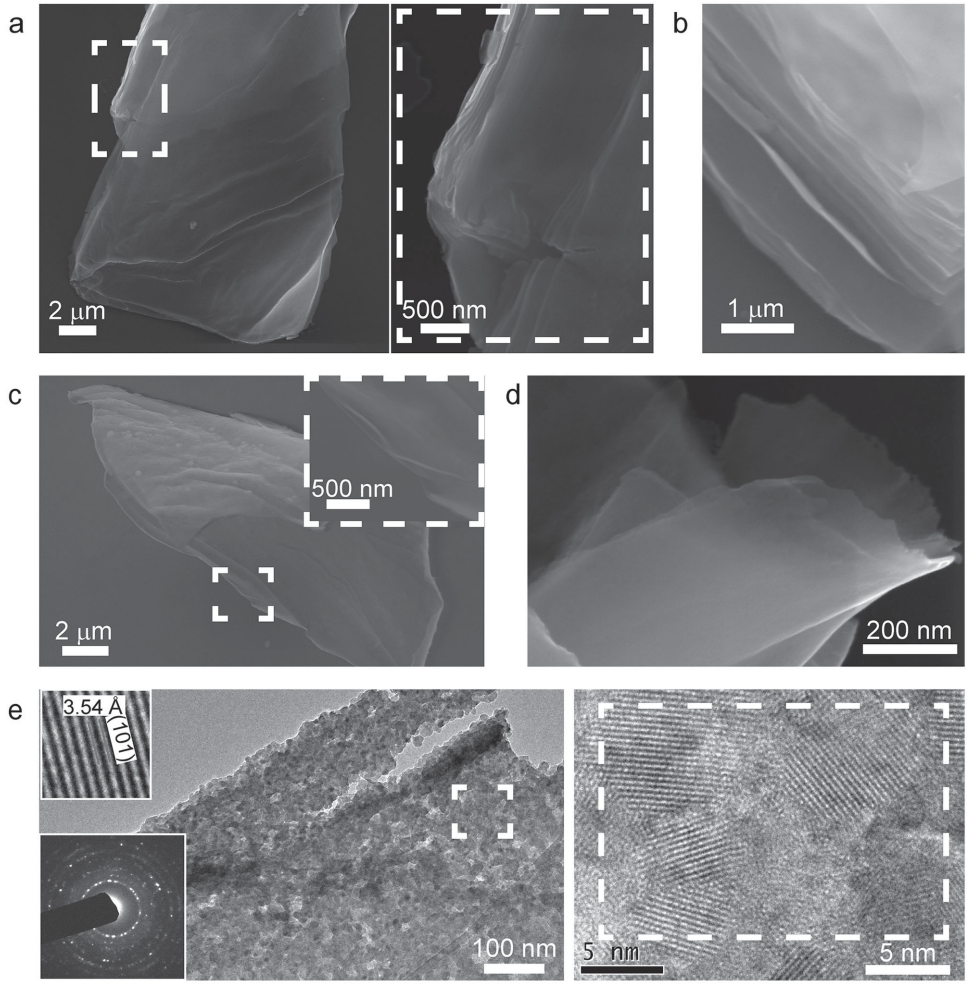

Figure 2. Electron microscope images of 2D TiO_2 nanolayers. a) SEM images of stacked nanolayers of TiO_2. b) Side view SEM image of stacked TiO_2 nanolayers. c) SEM image of double layers of TiO_2 nanolayers. d) SEM image of separated TiO_2 nanolayers showing highly flexible layers. e) TEM images and SAED pattern of TiO_2 nanolayer.

stratagem with different precursor solutions. Detailed methods and conditions for each material were shown in the Experimental Section.

2.3. Results and Discussions

The microstructure and surface morphology of ONLs were observed by scanning electron microscopy (SEM) and transmission electron microscopy (TEM) analysis. **Figure 2** shows the SEM images of TiO_2 nanolayers after a complete removal of GO templates. Obviously, the layered structure of GO paper was copied to oxide materials. Uniform and smooth ultrathin inorganic layers remained after a complete removal of rGO and stacked to form a large and thick membrane (Figure 2a and b). According to TEM, selected area electron diffraction (SAED), XRD, and energy dispersive X-ray spectroscopy (EDS) analysis (Figure 2e, and Figures S4–S6, Supporting Information), the nanolayer is polycrystalline anatase TiO_2. The stacked nanolayers can be easily separated into single or few-layers nanosheets by sonication in its aqueous solution. Figure 2c shows separated TiO_2 nanolayers spreading on the surface of silicon wafer. Importantly, the oxide nanolayers show superior mechanical flexibility as shown in Figure 2d. The flexible nature of ONLs can be understood by considering its nanocrystalline structure and 2D-layered morphology. The thickness of TiO_2 nanolayer was measured by atomic force microscopy (AFM) and by taking TEM from cross section. The thickness of the TiO_2 ONL is less than 5 nm according to AFM image (**Figure 3**a). In addition, AFM image of stacked TiO_2 nanolayers is shown in Figure S7 (Supporting Information). The first step (4.90 nm) indicates single TiO_2 layer and the second step (14.3 nm) indicates a few stacked oxide layers. Figure S6 (Supporting Information) shows the cross section TEM image of a single TiO_2 layer. The thickness of this sheet is measured to be 5 nm, which agrees well with the results of AFM. On the other hand, XRD profile analysis (Figure S4, Supporting Information) shows that the mean crystallite size of TiO_2 nanolayer is about 27.2 nm. These results indicate that the TiO_2 nanolayer would be composed of 2D crystallite. In order to further understand the mechanism for the formation of oxide nanolayers, we analyzed the structures of intermediate steps based on cross section SEM and Raman spectroscopy. Figure S8

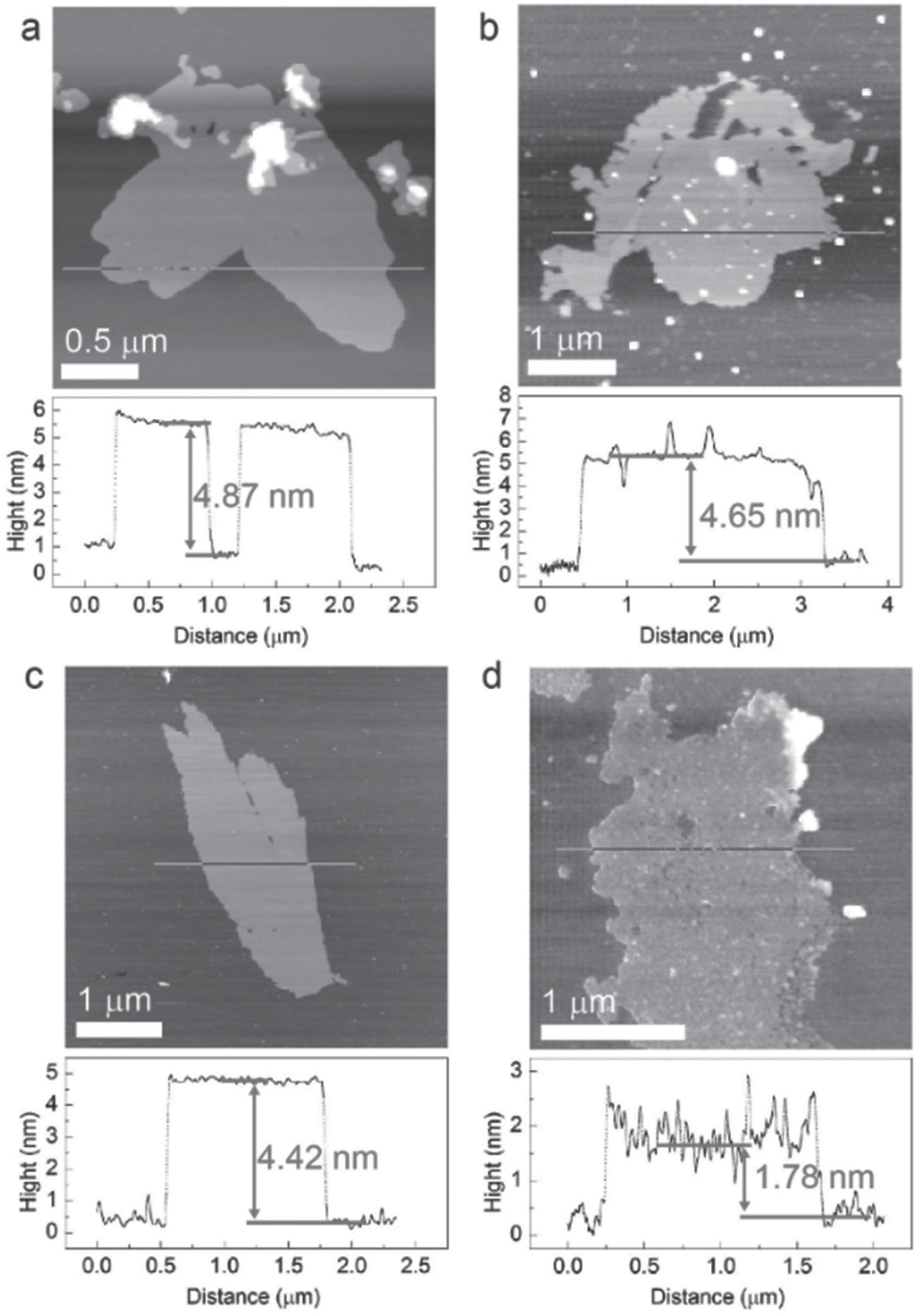

Figure 3. AFM images of 2D oxide nanolayers. AFM images of single nanolayer structure of a) TiO_2, b) ZnO, c) Fe_2O_3, and d) SiO_2.

(Supporting Information) shows the cross section SEM images of GO sheet before and after soaking in TiO_2 precursor solution at the same position. It can be seen that the thickness of GO sheet increased from 2.81 to 4.58 μm after soaking into the precursor solution and drying, clearly indicating that the precursor solids inserted into the interlayer spaces between GO layers expand the gap between GO. Figure S9 (Supporting Information) exhibits Raman spectra of intermediate steps. Alternate layer-by-layer sheet of TiO_2 and rGO, and TiO_2 ONL have anatase phase peaks at around 143, 395, 514, 636 cm^{-1}. The d-band (1350 cm^{-1}) and g-band (1600 cm^{-1}) from graphite and its defect structure have not been observed at TiO_2 nanolayers. These results clearly suggest a full conversion of the precursor into TiO_2 and a complete removal of carbon after annealing in air. The decomposition process is also studied by thermal analysis. We observed the decomposition of GO by thermal gravimetric analysis (TGA) at 600 °C

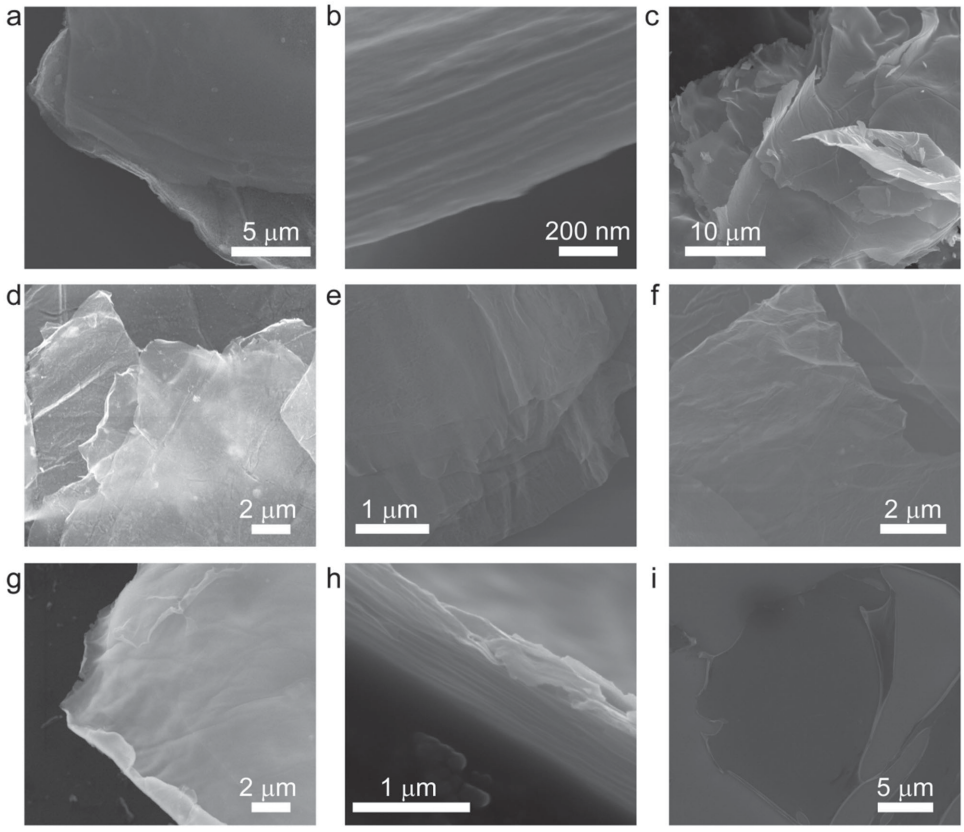

Figure 4. Electron microscope images of 2D oxide nanolayers. a,b,d,e,g,h) SEM images of stacked ONLs: a,d,g) Top view SEM images and b,e,h) side view SEM images of a,b) ZnO, d,e) Fe_2O_3, and g,h) SiO_2 ONL sheets. c,f,i) SEM images of separated nanolayers of c) ZnO, f) Fe_2O_3, and i) SiO_2.

for 1 h in air (Figure S10, Supporting Information). The decrease of sample weight stopped right after temperature reaching 600 °C in TGA measurement.

In principle, the synthesis of ONLs in the gaps between GO can be extended to obtain oxide materials beyond TiO_2. As examples, we fabricated ZnO, Fe_2O_3, and SiO_2 nanolayers by soaking GO paper in corresponding precursor solutions and subsequent calcinations (experimental detail in the Experimental section). Oxide nanolayers can be easily obtained using this strategy as shown in **Figure 4**. These 2D nanomaterials also can be separated into single or few-layers nanosheets by a simple ultrasonication method, as shown in the SEM images in Figure 4c,f,i. Figure 3 shows the AFM images of each thin ONL. The measured thicknesses of ZnO, Fe_2O_3, and SiO_2 layers are only about 4.65, 4.42, and 1.78 nm, respectively. Additionally, to research the thickness distribution of ONLs synthesized by this strategy, we easily calculated the average thickness of ten pieces of ZnO nanolayers, which is 3.38 ± 0.74 nm (Figure S11, Supporting Information). The thickness of all the measured layers is less than 5 nm. According to XRD patterns and their diffraction profile analysis (Figure S4, Supporting Information), the ZnO and Fe_2O_3 ONLs are comprised of well-crystallized wurtzite and hematite polycrystals whose mean crystallite sizes are 17.2 and 31.4 nm, respectively, which indicate that these ONLs would also be composed of 2D crystallites as well as TiO_2 nanolayer. In contrast to the TiO_2, ZnO, and Fe_2O_3 ONLs, SiO_2 ONLs show amorphous structure (Figure S4, Supporting Information).

2.4. ONL for Battery Electrode Applications

The synthesized ONL nanomaterials are promising for multiple applications, for example, photocatalyst, flexible sensor, solar cells, gas separation, electrodes for super capacitors, and batteries.[3,12,15,28,44] Functional oxides with graphene-like 2D nanostructure are particularly interesting for Li-ion battery electrode application due to following reasons: (1) the high surface to volume ratio: BET surface area 166 $m^2\ g^{-1}$ (Figure S12, Supporting Information) and open edge geometry represent an ideal 2D structure which can provide fast and efficient charge transfer channels; (2) the 2D geometry of nanolayers is beneficial to the effective electric contact inside battery electrode. Due to a large contact area, the contact between nanolayer/electrolyte, nanolayer/nanolayer, nanolayer/current collector, and nanolayer/conductive additives is expected to be greatly enhanced; (3) the flexible oxide 2D nanolayers can tolerate large strain associated with battery reactions. Considering these, we proposed that transition metal oxide nanolayers can serve as high-performance electrode for Li-ion batteries. Fe_2O_3 nanolayers have been assembled into battery electrode as active

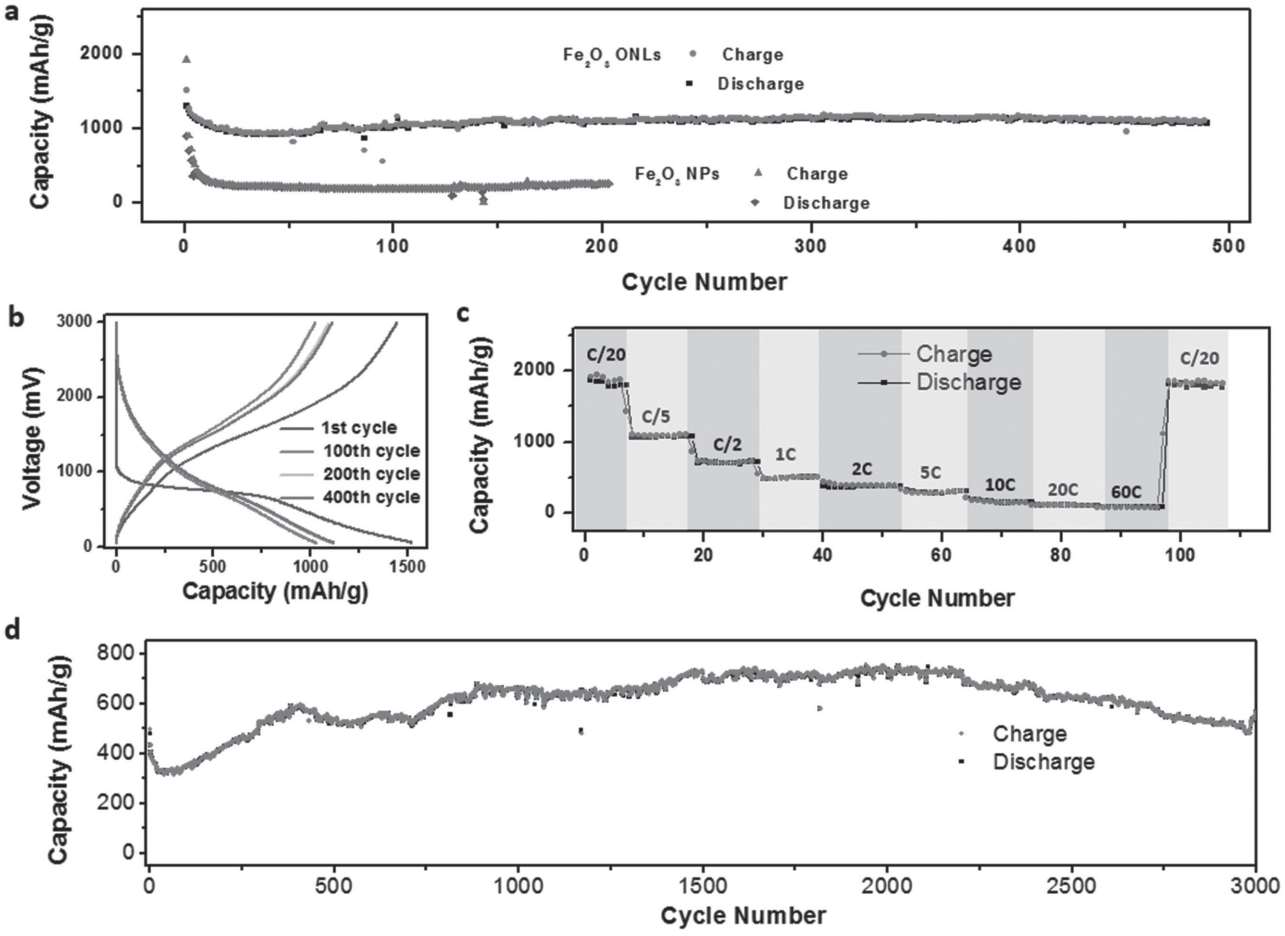

Figure 5. Electrochemical characteristics. a) Electrochemical cycling performance of the Fe_2O_3 ONL electrode under deep charge/discharge cycles from 3 to 0 V with a charge/discharge current of 1 A g^{-1}, showing stable capacity of 1000 mAh g^{-1} after 500 cycles (red line). Electrochemical cycling of control samples of Fe_2O_3 nanoparticle electrode is compared in the figure. b) Galvanostatic charge/discharge profiles plotted for the 1st, 100th, 200th, and 400th cycles. c) Capacity of Fe_2O_3 ONL electrode cycled at various rates from C/20 to 60C. d) Lithiation/delithiation capacity of Fe_2O_3 ONL electrodes cycled at 6 A g^{-1} for 3000 cycles. a–d) All electrochemical cycling measurements were carried out at room temperature in two-electrode 2032 coin-type half-cells.

lithium-ion storage materials. The electrochemical cycling performance of the electrodes has been evaluated using deep charge/discharge galvanostatic cycling from 3 to 0 V (**Figure 5**). The first discharge has a long plateau around 0.8 V, which corresponds to the lithiation potential of pure Fe_2O_3 (Figure 5b). At a charge/discharge current of 1.0 A g^{-1}, the Fe_2O_3 ONL electrode exhibits a relatively stable reversible lithium capacity of around 1000 mAh g^{-1} for more than 500 deep cycles (Figure 5a). In comparison, the Fe_2O_3 nanoparticle electrode loses more than 40% of its initial capacity and decreased its capacity to around 300 mAh g^{-1} after being cycled 100 times (Figure 5a). In addition, the 2D Fe_2O_3 nanomaterials hold high surface area as well as short channels for fast electron and ion transport, thereby enabling outstanding rate capability as shown in Figure 5c. Clearly, Li^+ ions can rapidly pass through the thin Fe_2O_3 layers even at high charge/discharge rates. To obtain long cycling results within a reasonable testing period, faster charge and discharge tests with deep cycling (3 to 0 V) were carried out. Figure 5d shows that at a high current density of 6.0 A g^{-1}, an electrode capacity of ≈500 mAh g^{-1} was still retained after 3000 cycles. This result clearly indicates its superior and stable cycling performance.

3. Conclusion

In conclusion, we have demonstrated a new strategy to synthesize 2D oxides inside GO paper gaps. This approach has multiple advantages. First, it applies for a large variety of oxide materials, while the existing exfoliation methods only work for 2D layers from originally layered materials. Second, ceramic and glassy ONLs can be controlled with thickness of less than a few nanometers and sizes of more than several micrometers. Finally, the approach constructs 2D oxides through only several facile solution based steps, therefore can be potentially adapted to larger scale productions. The ONL structures not only help to improve performance in lithium-ion battery electrodes, they are also interesting for photocatalyst and flexible electronics. More importantly, our results open a window to insight the tiny 2D gaps in GO paper, where huge potential exists.

4. Experimental Section

Reagents: GO dispersion solution (3 mg mL^{-1}) was purchased from Hefei Ke Jing Materials Technology Co., Ltd. Tetrabutyl titanate and zinc acetate dihydrate were purchased from Beijing Yili Fine Chemical Co., Ltd. Tetraethyl orthosilicate and iron nitrate nonahydrate were purchased from Tianjin Damao Chemical Reagent Factory. All regents were used as received without further purification.

Preparation of GO Paper: GO paper was prepared by dropping 150 µL GO dispersion solution on a silicon wafer with a size of $10 \times 10 \times 0.5$ mm (Institute of Coal Chemistry, Chinese Academy of Sciences) and drying at 80 °C.

Synthesis of TiO_2 Nanosheets: Tetrabutyl titanate (TBT, 3.50 g) was added to dehydrated ethanol (3.50 g) during vigorous stirring at room temperature. After stirring, GO sheet was immersed in TBT uniform solution (1.30 mol L^{-1}) for 24 h. After immersion, GO sheet was washed by dehydrated ethanol two times and dried at 80 °C for 3 h. Then, GO sheet was calcined in a tube furnace (OTF-1200-X, MTI Co.) with argon atmosphere at 500 °C for 1 h at a heating rate of 5 °C min^{-1}. The calcined sheet was added to ethanol and exfoliated by sonication for 20 min. Finally, the slurry was casted on a silicon wafer and calcined in air atmosphere at 600 °C for 1h at a heating rate of 5 °C min^{-1}.

Synthesis of ZnO Nanosheets: Zinc acetate dihydrate ($ZnAc_2{\cdot}2H_2O$, 1.10 g) was added to deionized water (9.88 g) during vigorous stirring at room temperature. After stirring, GO sheet was immersed in zinc acetate uniform solution (10 wt%) for 24 h. After immersion, GO sheet was washed by deionized water two times and dried at 80 °C for 3 h. Then, GO sheet was calcined in a tube furnace with argon atmosphere at 500 °C for 1 h at a heating rate of 5 °C min^{-1}. The calcined sheet was added to ethanol and exfoliated by sonication for 20 min. Finally, the slurry was casted on a silicon wafer and calcined in air atmosphere at 600 °C for 1 h at a heating rate of 5 °C min^{-1}.

Synthesis of Fe_2O_3 Nanosheets: Iron nitrate nonahydrate ($Fe(NO_3)_3{\cdot}9H_2O$, 1.40 g) was added to deionized water (7.00 g) during vigorous stirring at room temperature. After stirring, GO sheet was immersed in iron nitrate uniform solution (10 wt%) for 24 h. After immersion, GO sheet was washed by deionized water two times and dried at 80 °C for 3 h. Then, GO sheet was calcined in a tube furnace with argon atmosphere at 600 °C for 1 h at a heating rate of 5 °C min^{-1}. The calcined sheet was added to ethanol and exfoliated by sonication for 20 min. Finally, the slurry was casted on silicon wafer and calcined in air atmosphere at 600 °C for 1 h at a heating rate of 5 °C min^{-1}.

Synthesis of SiO_2 Nanosheets: Tetraethyl orthosilicate (TEOS, 2.70 g) was added to dehydrated ethanol (5.63 g) during vigorous stirring at room temperature. After stirring, GO sheet was immersed in TEOS uniform solution (1.30 mol L^{-1}) for 24 h. After immersion, GO sheet was washed by dehydrated ethanol two times and dried at 80 °C for 3 h. Then, GO sheet was calcined in a tube furnace with argon atmosphere at 500 °C for 1 h at a heating rate of 5 °C min^{-1}. The calcined sheet was added to ethanol and exfoliated by sonication for 20 min. Finally, the slurry was casted on a silicon wafer and calcined in air atmosphere at 600 °C for 1 h at a heating rate of 5 °C per min.

Characterization: SEM observation was conducted using MERLIN VP Compact, Carl Zeiss, and MIRA 3 LMH, TESCAN. TEM observation was conducted using JEM-2010, JEOL Corp. TEM sample was prepared by dispersion in ethanol using slight sonication of produced nanolayers and drop casting onto carbon-coated Cu grids. AFM observation was conducted using SPA300HV, Seiko Instruments, Inc., and MFP-3D, Asylum Research. AFM samples were prepared by dispersion in ethanol using slight sonication of produced nanolayers and drop casting onto a silicon wafer. XRD and Raman measurement were conducted using D/max 2500V, Rigaku, and LabRAM HR, HORIBA Jobin Yvon, respectively. Their samples were synthesized by directly calcined process from argon atmosphere to air atmosphere without sonication at same temperature with each nanosheet synthesis. TGA measurement was performed using STA 409 PC, Netzsch at a heating rate of 5 °C min^{-1} in Air/Ar mixuture gas atmosphere (3:1 v/v). Nitrogen adsorption measurements were conducted using Autosorb iQ2, Quantachrome at 77 K.

Electrode Fabrication and Electrochemical Measurement: Fe_2O_3 nanolayers were synthesized by directly calcined process from argon atmosphere to air atmosphere without sonication and Fe_2O_3 nanoparticles (MTI Co.) were used as the anode material of lithium-ion battery. Electrochemical measurements of the electrode were performed with LIR2032 Coin-type half-cells assembled in an argon-filled glove box (MB200MOD, CENN Nanocenter). A 25 µm thick microporous polypropylene membrane was applied as the separator (Asahi Kasei), 1 M $LiPF_6$ in ethylene carbonate/diethyl carbonate/fluoroethylene carbonate (1:1:0.04 v/v/v (Ferro Co.)) was used as the electrolyte, and Li foil (MTI Co.) was used as the counter electrode. All electrochemical measurements were carried out at room temperature. We evaluated the electrochemical performance between 0 and 3 V versus Li^+/Li under various rates (BS-9300R/10V2A 8 channels battery analyzer, MTI Co.).

Supporting Information

Supporting Information is available from the Wiley Online Library or from the author.

Acknowledgements

Y.S. and X.L. contributed equally to this work. This work was supported by the National Basic Research of China (Grant Nos. 2015CB932500 and 2013CB632702) and the National Science Foundation of China (Grant No. 51302141). H.W. acknowledges the support from the 1000 Youth Talents Plan of China.

Received: April 4, 2015
Revised: July 10, 2015
Published online: August 11, 2015

[1] A. K. Geim, K. S. Novoselov, *Nat. Mater.* **2007**, *6*, 183.
[2] W. C. Ren, H. M. Cheng, *Nat. Nanotechnol.* **2014**, *9*, 726.
[3] W. Z. Wu, L. Wang, Y. L. Li, F. Zhang, L. Lin, S. M. Niu, D. Chenet, X. Zhang, Y. F. Hao, T. F. Heinz, J. Hone, Z. L. Wang, *Nature* **2014**, *514*, 470.
[4] Z. L. Ye, T. Cao, K. O'Brien, H. Y. Zhu, X. B. Yin, Y. Wang, S. G. Louie, X. Zhang, *Nature* **2014**, *513*, 214.
[5] M. S. Xu, T. Liang, M. M. Shi, H. Z. Chen, *Chem. Rev.* **2013**, *113*, 3766.
[6] K. S. Novoselov, D. Jiang, F. Schedin, T. J. Booth, V. V. Khotkevich, S. V. Morozov, A. K. Geim, *Proc. Natl. Acad. Sci. USA* **2005**, *102*, 10451.
[7] O. V. Yazyev, Y. P. Chen, *Nat. Nanotechnol.* **2014**, *9*, 755.
[8] W. J. Roth, P. Nachtigall, R. E. Morris, J. Cejka, *Chem. Rev.* **2014**, *114*, 4807.
[9] S. Z. Butler, S. M. Hollen, L. Y. Cao, Y. Cui, J. A. Gupta, H. R. Gutierrez, T. F. Heinz, S. S. Hong, J. X. Huang, A. F. Ismach, E. Johnston-Halperin, M. Kuno, V. V. Plashnitsa, R. D. Robinson, R. S. Ruoff, S. Salahuddin, J. Shan, L. Shi, M. G. Spencer, M. Terrones, W. Windl, J. E. Goldberger, *ACS Nano* **2013**, *7*, 2898.
[10] K. J. Koski, Y. Cui, *ACS Nano* **2013**, *7*, 3739.
[11] M. Chhowalla, H. S. Shin, G. Eda, L. J. Li, K. P. Loh, H. Zhang, *Nat. Chem.* **2013**, *5*, 263.
[12] O. Lopez-Sanchez, D. Lembke, M. Kayci, A. Radenovic, A. Kis, *Nat. Nanotechnol.* **2013**, *8*, 497.
[13] J. W. Colson, A. R. Woll, A. Mukherjee, M. P. Levendorf, E. L. Spitler, V. B. Shields, M. G. Spencer, J. Park, W. R. Dichtel, *Science* **2011**, *332*, 228.

[14] M. Heyde, *Science* **2013**, *342*, 201.
[15] Y. Peng, Y. S. Li, Y. J. Ban, H. Jin, W. M. Jiao, X. L. Liu, W. S. Yang, *Science* **2014**, *346*, 1356.
[16] X. B. Yin, Z. L. Ye, D. A. Chenet, Y. Ye, K. O'Brien, J. C. Hone, X. Zhang, *Science* **2014**, *344*, 488.
[17] J. Zhao, Q. M. Deng, A. Bachmatiuk, G. Sandeep, A. Popov, J. Eckert, M. H. Rummeli, *Science* **2014**, *343*, 1228.
[18] M. P. Boneschanscher, W. H. Evers, J. J. Geuchies, T. Altantzis, B. Goris, F. T. Rabouw, S. A. P. van Rossum, H. S. J. van der Zant, L. D. A. Siebbeles, G. Van Tendeloo, I. Swart, J. Hilhorst, A. V. Petukhov, S. Bals, D. Vanmaekelbergh, *Science* **2014**, *344*, 1377.
[19] K. Celebi, J. Buchheim, R. M. Wyss, A. Droudian, P. Gasser, I. Shorubalko, J. I. Kye, C. Lee, H. G. Park, *Science* **2014**, *344*, 289.
[20] J. M. Yuk, J. Park, P. Ercius, K. Kim, D. J. Hellebusch, M. F. Crommie, J. Y. Lee, A. Zettl, A. P. Alivisatos, *Science* **2012**, *336*, 61.
[21] Z. Q. Sun, T. Liao, Y. H. Dou, S. M. Hwang, M. S. Park, L. Jiang, J. H. Kim, S. X. Dou, *Nat. Commun.* **2014**, *5*, 3818.
[22] F. Torrisi, J. N. Coleman, *Nat. Nanotechnol.* **2014**, *9*, 738.
[23] B. X. Mi, *Science* **2014**, *343*, 740.
[24] R. Addou, A. Dahal, M. Batzill, *Nat. Nanotechnol.* **2013**, *8*, 41.
[25] L. K. Li, Y. J. Yu, G. J. Ye, Q. Q. Ge, X. D. Ou, H. Wu, D. L. Feng, X. H. Chen, Y. B. Zhang, *Nat. Nanotechnol.* **2014**, *9*, 372.
[26] J. W. Colson, W. R. Dichtel, *Nat. Chem.* **2013**, *5*, 453.
[27] G. Fiori, F. Bonaccorso, G. Iannaccone, T. Palacios, D. Neumaier, A. Seabaugh, S. K. Banerjee, L. Colombo, *Nat. Nanotechnol.* **2014**, *9*, 768.
[28] M. F. El-Kady, V. Strong, S. Dubin, R. B. Kaner, *Science* **2012**, *335*, 1326.
[29] H. H. Duan, N. Yan, R. Yu, C. R. Chang, G. Zhou, H. S. Hu, H. P. Rong, Z. Q. Niu, J. J. Mao, H. Asakura, T. Tanaka, P. J. Dyson, J. Li, Y. D. Li, *Nat. Commun.* **2014**, *5*, 3093.
[30] C. L. Tan, H. Zhang*Chem. Soc. Rev.* **2015**, *44*, 2713.
[31] M. R. Lukatskaya, O. Mashtalir, C. E. Ren, Y. Dall'Agnese, P. Rozier, P. L. Taberna, M. Naguib, P. Simon, M. W. Barsoum, Y. Gogotsi, *Science* **2013**, *341*, 1502.
[32] O. Mashtalir, M. Naguib, V. N. Mochalin, Y. Dall'Agnese, M. Heon, M. W. Barsoum, Y. Gogotsi, *Nat. Commun.* **2013**, *4*, 1716.
[33] J. A. Rogers, M. G. Lagally, R. G. Nuzzo, *Nature* **2011**, *477*, 45.
[34] B. B. Lakshmi, C. J. Patrissi, C. R. Martin, *Chem. Mat.* **1997**, *9*, 2544.
[35] D. Li, Y. N. Xia, *Adv. Mater.* **2004**, *16*, 1151.
[36] D. A. Dikin, S. Stankovich, E. J. Zimney, R. D. Piner, G. H. B. Dommett, G. Evmenenko, S. T. Nguyen, R. S. Ruoff, *Nature* **2007**, *448*, 457.
[37] R. K. Joshi, P. Carbone, F. C. Wang, V. G. Kravets, Y. Su, I. V. Grigorieva, H. A. Wu, A. K. Geim, R. R. Nair, *Science* **2014**, *343*, 752.
[38] H. W. Kim, H. W. Yoon, S. M. Yoon, B. M. Yoo, B. K. Ahn, Y. H. Cho, H. J. Shin, H. Yang, U. Paik, S. Kwon, J. Y. Choi, H. B. Park, *Science* **2013**, *342*, 91.
[39] O. C. Compton, S. T. Nguyen, *Small* **2010**, *6*, 711.
[40] L. Qiu, J. Z. Liu, S. L. Y. Chang, Y. Z. Wu, D. Li, *Nat. Commun.* **2012**, *3*, 1241.
[41] D. Li, M. B. Muller, S. Gilje, R. B. Kaner, G. G. Wallace, *Nat. Nanotechnol.* **2008**, *3*, 101.
[42] D. Li, R. B. Kaner, *Science* **2008**, *320*, 1170.
[43] V. C. Tung, M. J. Allen, Y. Yang, R. B. Kaner, *Nat. Nanotechnol.* **2009**, *4*, 25.
[44] X. W. Yang, C. Cheng, Y. F. Wang, L. Qiu, D. Li, *Science* **2013**, *341*, 534.
[45] L. Stobinski, B. Lesiak, A. Malolepszy, M. Mazurkiewicz, B. Mierzwa, J. Zemek, P. Jiricek, I. Bieloshapka, *J. Electron Spect. Rel. Phen.* **2014**, *195*, 145.